Supplemental Material

To show the performance variation under the increasing noise level, an incomplete (half part of) cube is synthesized as the ground truth model with the known convex features. Meanwhile, different levels of Gaussian noise are imposed on this point cloud. We implement both APSS and NRLC algorithms on this original and the noisy models. We record the mean curvature of each point for the APSS method and the parallel component of each feature vector for the NRLC algorithm. These two quantities are also visualized in the second and third columns of Fig. 1.

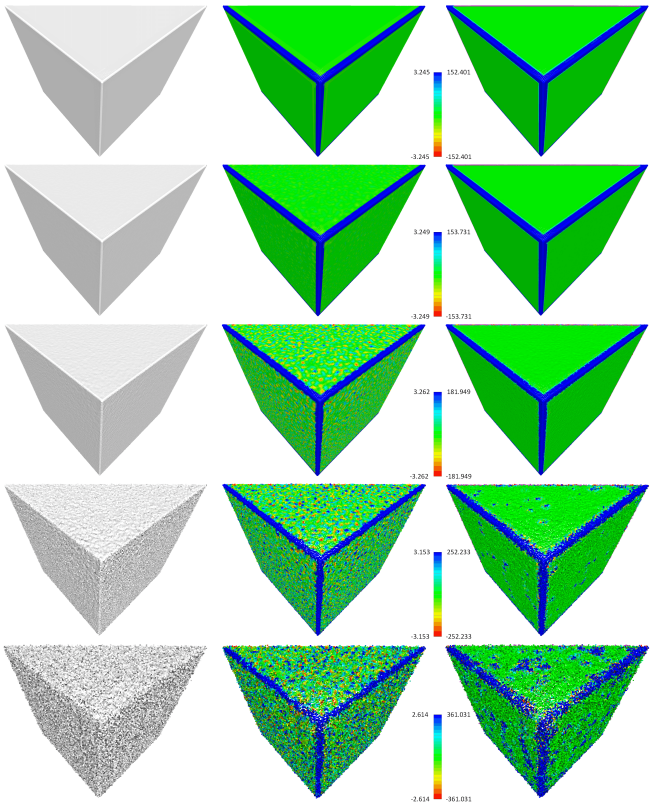

Fig. 1. Visualizing the shape variations on a half part cube and its noisy models. From top to bottom are the standard cube and cubes with different noise levels, controlled by the Gaussian kernel with the standard deviation σ (0.01, 0.03, 0.08, 0.20). For each case, from left to right are the original model, the results of APSS and NRLC.

We calculate the differences for the parallel component of the feature vector (NRLC) and the mean curvature (APSS) between the ground truth and each noisy model. The average difference is defined as Eq. (1),

$$D_f(\sigma) = \frac{1}{m_f} \sum_{p_i \in P_f} \frac{I_i^{(0)} - I_i^{(\sigma)}}{avg\_I_f^{(0)}} \tag{1}$$

where $I_i^{(0)}$ is the parallel component of the feature vector for NRLC (or the mean curvature for APSS) on the ground truth model for the i-th point and $I_i^{(\sigma)}$ is the same quantity in the noisy model with noise standard deviation σ. $avg\_I_f^{(0)}$ is the average of the parallel component of the feature vector (NRLC) or the average of the mean curvature (APSS) on the ground truth model. The average differences are computed for both the APSS and NRLC methods on specified point classes f (convex and nonfeature). m_f is the point number of specified class f. The average differences for different point classes produced by both methods on models with different noise levels are reported in TABLE 1.

We also plot these average differences of noisy models with increasing σ to show the noise resistance of both methods in Fig. 2.

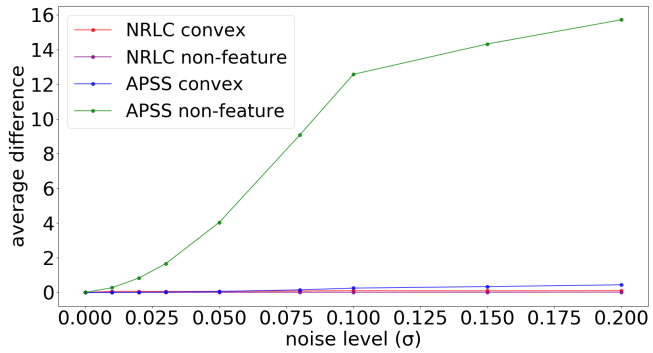

(a) Average differences of convex and nonfeature classes for APSS and NRLC.

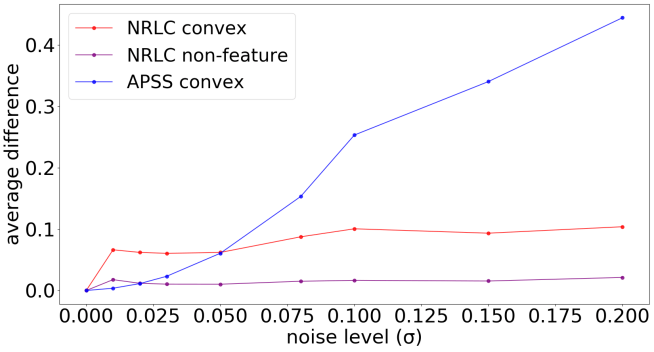

(b) Zoomed-in view of the convex and nonfeature lines of NRLC and the convex line of APSS.

Fig. 2. Variation of the average differences of APSS and NRLC on convex and nonfeature classes as the noise standard deviation increases.

Fig. 3 and Fig. 4 demonstrate the NRLC recognized geometric features on the bunny and relief, respectively. The refined feature sets are produced by combining the

TABLE 1
The statistics of the average differences between the noisy models and the ground truth for APSS and NRLC on two point classes (convex and nonfeature)

NL	APSS		NRLC	
(Noise Level)	Convex	Nonfeature	Convex	Nonfeature
0.01	0.0037	0.2764	0.0663	0.0177
0.02	0.0113	0.8331	0.0620	0.0117
0.03	0.0232	1.6591	0.0605	0.0103
0.05	0.0607	4.0423	0.0620	0.0102
0.08	0.1532	9.0726	0.0875	0.0151
0.10	0.2532	12.5706	0.1005	0.0165
0.15	0.3403	14.3212	0.0934	0.0155
0.20	0.4443	15.7180	0.1038	0.0213

assimilation and dissimilation operations.

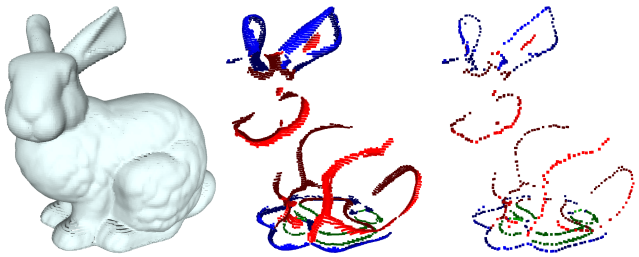

Fig. 3. NRLC generates geometric feature sets (middle) for the bunny model (left). The thin feature sets (right) are created by dissimilating those thick features.

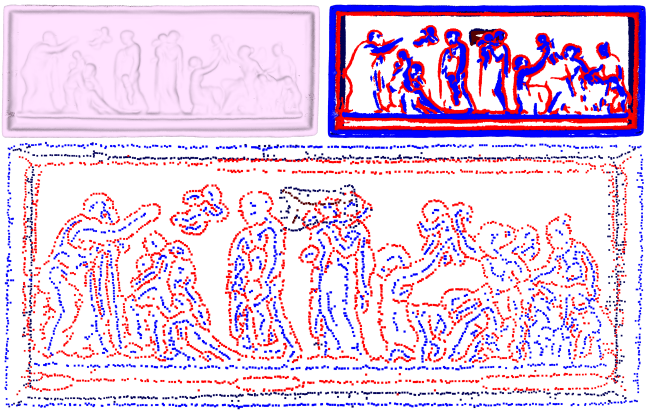

Fig. 4. NRLC produces geometric features (top-right) for a relief point cloud (top-left). The thin relief features (bottom) are generated by first implementing a set of assimilations and then enforcing another set of dissimilation operations on the thick feature sets.

To further show the feature identification capability, we implement NRLC on two additional single view surfaces SVS3 (Fig. 5) and SVS4 (Fig. 6) and two indoor point clouds Scene3 (Fig. 7) and Scene4 (Fig. 8).

Another set of comparison experiments on the LiDAR building point cloud is implemented to illustrate the generalization capability of the proposed NRLC; see the results in Fig. 9. The interference of the outliers for feature identification of NRLC is also explained in Fig. 10.

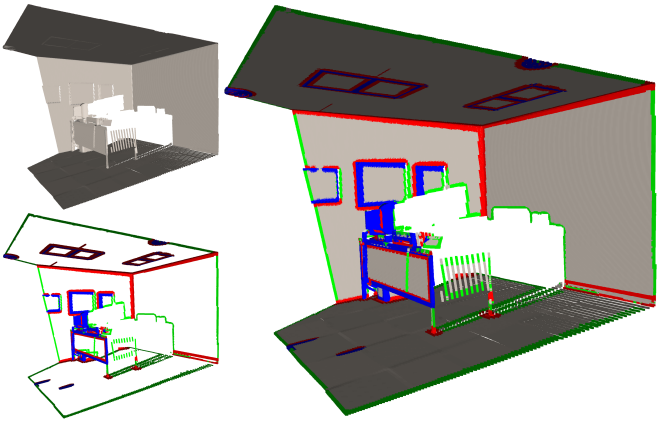

Fig. 5. NRLC works on the third single-view surface SVS3. Top-left: the input point cloud. Right: NRLC-identified result. Bottom-left: feature sets.

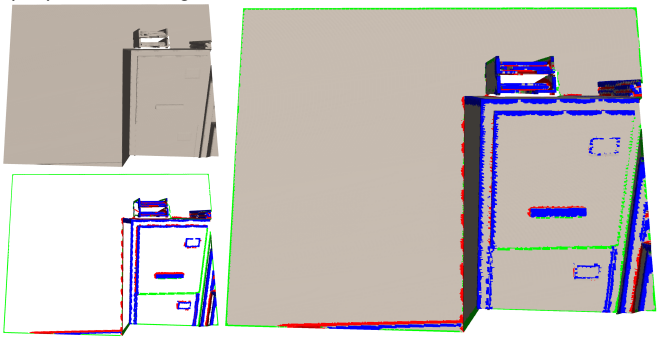

Fig. 6. Implementing NRLC on the fourth single-view surface SVS4. Top-left: the input point cloud. Right: NRLC-identified result. Bottom-left: feature sets.

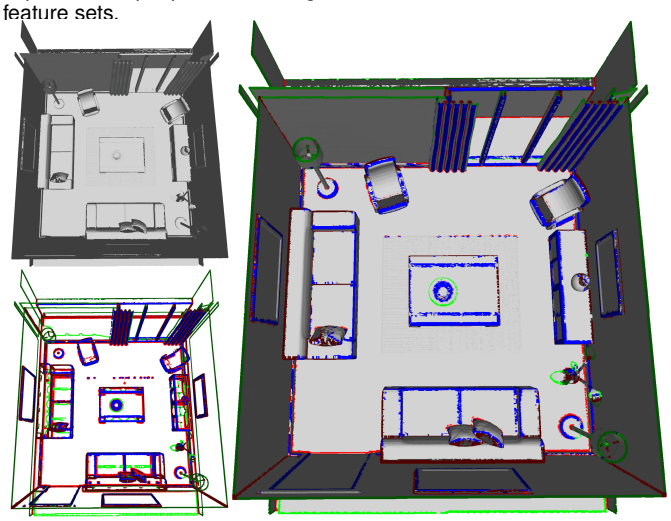

Fig. 7. Geometric features produced by NRLC on a synthetic living room Scene3. Top-left: the input point cloud. Right: NRLC identified result. Bottom-left: feature sets.

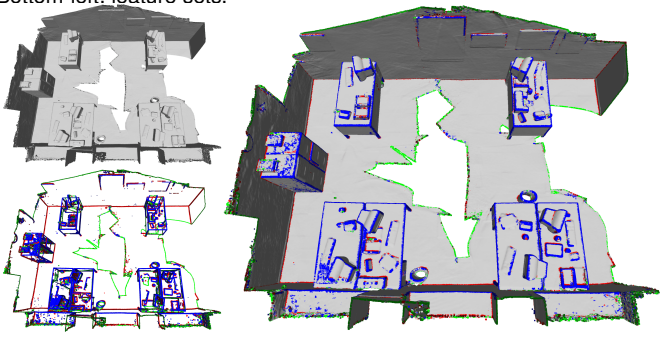

Fig. 8. The geometric features produced by NRLC on an incomplete large office with heavy noise Scene4. Top-left: the input model. Right: NRLC-identified result. Bottom-left: feature sets.

Fig. 9. Comparison experiment between F3D [42], PCA [32], and NRLC on the second LiDAR building point cloud. From top to bottom, these figures are the input model, feature sets generated by F3D, PCA and NRLC.

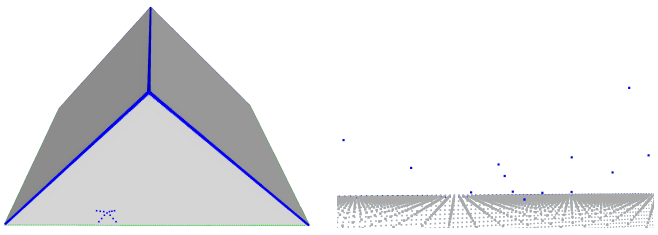

(a) (b)

Fig. 10. Geometric feature identification for point clouds with outliers. (a) and (b) are the top view and side view of the tested result, respectively.